

Modeling of the influence of coupling in optical microfiber resonators

Wei Guo, Ye Chen, Fei Xu,¹ and Yan-qing Lu²

National Laboratory of Solid State Microstructures and College of Engineering and Applied Sciences Nanjing University, Nanjing 210093, China

¹feixu@nju.edu.cn

²yqlu@nju.edu.cn

Abstract: By modifying the resonance condition of optical microfiber resonator while considering the strong coupling effect, we theoretically investigate the influence of coupling on the resonant wavelength and refractive index sensitivity, and compare our results with the previously published results. Numerical calculation shows significant difference in resonant wavelength and sensitivity for different coupling strengths. By considering coupling effect, the resonant peak position can be shifted as far as 3.89 nm and the sensitivity can be modified by as much as 83 nm/RIU. This suggests a method to tune the resonant wavelength and sensitivity, by varying the pitch and the coupling between two adjacent microfibers in the coupling area.

©2012 Optical Society of America

OCIS codes: (060.2340) Fiber optics components; (230.5750) Resonators; (060.2370) Fiber optics sensors.

References and links

1. G. Brambilla, "Optical fiber nanowires and microwires: a review," *J. Opt.* **12**(4), 043001 (2010).
2. L. M. Tong, R. R. Gattass, J. B. Ashcom, S. L. He, J. Y. Lou, M. Y. Shen, I. Maxwell, and E. Mazur, "Subwavelength-diameter silica wires for low-loss optical wave guiding," *Nature* **426**(6968), 816–819 (2003).
3. L. Tong, "Brief introduction to optical microfibers and nanofibers," *Front. Optoelectron. China* **3**(1), 54–60 (2010).
4. G. Brambilla, V. Finazzi, and D. J. Richardson, "Ultra-low-loss optical fiber nanotapers," *Opt. Express* **12**(10), 2258–2263 (2004).
5. G. Brambilla, F. Xu, P. Horak, Y. Jung, F. Koizumi, N. P. Sessions, E. Koukharenko, X. Feng, G. S. Murugan, J. S. Wilkinson, and D. J. Richardson, "Optical fiber nanowires and microwires: fabrication and applications," *Adv. Opt. Photon.* **1**(1), 107–161 (2009).
6. K. S. Lim, S. W. Harun, S. S. A. Damanhuri, A. A. Jasim, C. K. Tio, and H. Ahmad, "Current sensor based on microfiber knot resonator," *Sens. Actuators A Phys.* **167**(1), 60–62 (2011).
7. X. Jiang, Y. Chen, G. Vienne, and L. Tong, "All-fiber add-drop filters based on microfiber knot resonators," *Opt. Lett.* **32**(12), 1710–1712 (2007).
8. F. Xu, V. Pruneri, V. Finazzi, and G. Brambilla, "An embedded optical nanowire loop resonator refractometric sensor," *Opt. Express* **16**(2), 1062–1067 (2008).
9. M. Sumetsky, Y. Dulashko, J. M. Fini, and A. Hale, "Optical microfiber loop resonator," *Appl. Phys. Lett.* **86**(16), 161108 (2005).
10. X. Guo and L. M. Tong, "Supported microfiber loops for optical sensing," *Opt. Express* **16**(19), 14429–14434 (2008).
11. T. Lee, N. G. R. Broderick, and G. Brambilla, "Berry phase magnification in optical microcoil resonators," *Opt. Lett.* **36**(15), 2839–2841 (2011).
12. F. Xu and G. Brambilla, "Demonstration of a refractometric sensor based on optical microfiber coil resonator," *Appl. Phys. Lett.* **92**, 101126 (2008).
13. F. Xu and G. Brambilla, "Embedding optical microfiber coil resonators in Teflon," *Opt. Lett.* **32**(15), 2164–2166 (2007).
14. M. Sumetsky, "Optical fiber microcoil resonators," *Opt. Express* **12**(10), 2303–2316 (2004).

15. J. Yongmin, G. S. Murugan, G. Brambilla, and D. J. Richardson, "Embedded optical microfiber coil resonator with enhanced high Q," *IEEE Photon. Technol. Lett.* **22**, 1638–1640 (2010).
 16. P. Pal and W. H. Knox, "Fabrication and characterization of fused microfiber resonators," *IEEE Photon. Technol. Lett.* **21**(12), 766–768 (2009).
 17. F. Xu, Q. Wang, J.-F. Zhou, W. Hu, and Y.-Q. Lu, "Dispersion study of optical nanowire microcoil resonators," *IEEE J. Sel. Top. Quantum Electron.* **17**(4), 1102–1106 (2011).
 18. K. Huang, S. Yang, and L. Tong, "Modeling of evanescent coupling between two parallel optical nanowires," *Appl. Opt.* **46**(9), 1429–1434 (2007).
 19. F. Xu, P. Horak, and G. Brambilla, "Conical and biconical ultra-high-Q optical-fiber nanowire microcoil resonator," *Appl. Opt.* **46**(4), 570–573 (2007).
 20. K. Okamoto, *Fundamentals of Optical Waveguides*, 2nd ed. (Elsevier, 2006).
-

1. Introduction

Subwavelength-diameter optical microfibers/nanofibers, have been extensively studied due to a number of interesting optical properties, such as their large evanescent field, low cost, low loss, and relative ease of coupling to single mode fibers [1–5]. Among such fibers, microfiber-based resonators (MFRs) have quickly emerged as an ideal sensor element and attracted a great deal of interest in the past few years because they can provide a large evanescent field for high sensitivity, high Q-factors for low detection thresholds, and correspondingly narrow resonant bandwidths for good wavelength selectivity. With the rapid development of fabrication technologies [4], many novel resonator structures based on microfibers have been reported, such as microfiber knot [6, 7], loop [8–10], and coil resonators [11–15]. These resonators have many potential applications in optical communications and sensing. A basic MFR includes a coupling region in which two pieces of microfiber are held close to each other by being twisted or fused together [16]. For most MFRs, the light propagating in the microfiber generates a large evanescent field, which interacts with the surrounding medium (the analyte). The cross-sectional geometry and the effective refractive index of the microfiber greatly influence the resonant wavelength and the sensitivity of MFRs. A smaller cross-section is preferred in MFRs to provide a larger evanescent field. However, the coupling effect between the two segments in the coupling region can be very strong [17, 18], especially when the diameter is small and the coupling length is relatively long. In previous works, the resonant wavelength and sensitivity have always been considered to depend only on the effective index of the microfiber and to be unrelated to the coupling. However, the coupling in the coupling region can be very strong because of the large evanescent field, sufficient interwaveguide coupling, and relatively long coupling length. It is possible for the strong coupling effect to greatly influence the resonance condition and sensitivity, and therefore, it should not be ignored. In this paper, we investigate the resonance condition and sensitivity of the MFR by considering the strong coupling effect and our simulation shows that the coupling effect has a great influence on the resonant peak position and the sensitivity of the MFR. The resonant peak position can be shifted as far as 3.89 nm and the sensitivity of the MFR can be modified by as much as 83 nm/RIU for certain parameter values. This is important and helpful for the design and applications of MFR sensors. In particular, the pitch between adjacent turns may change in response to external vibration or pressure applied to a microfiber coil resonator (MCR) coiled around a rod because of its unique 3D geometry. This suggests that we can use the MCR as a vibration sensor and also the alternative tuning technique of controlling the pitch and coupling strength.

2. Resonator structure and numerical model

Figure 1(a) shows a diagram of a typical MFR, which usually has a coupling region where two pieces of microfiber are in close proximity to each other. The pitch between the two pieces of microfiber is fixed and it is not possible to change it in a loop or knot resonator. However, it is

easy to tune it in an MCR. In this paper, for simplicity, we mainly consider the loop/knot MFR and the two-turn MCR with simple two-wave coupling equations, which are very similar and agree with the model, as shown in Fig. 1(a).

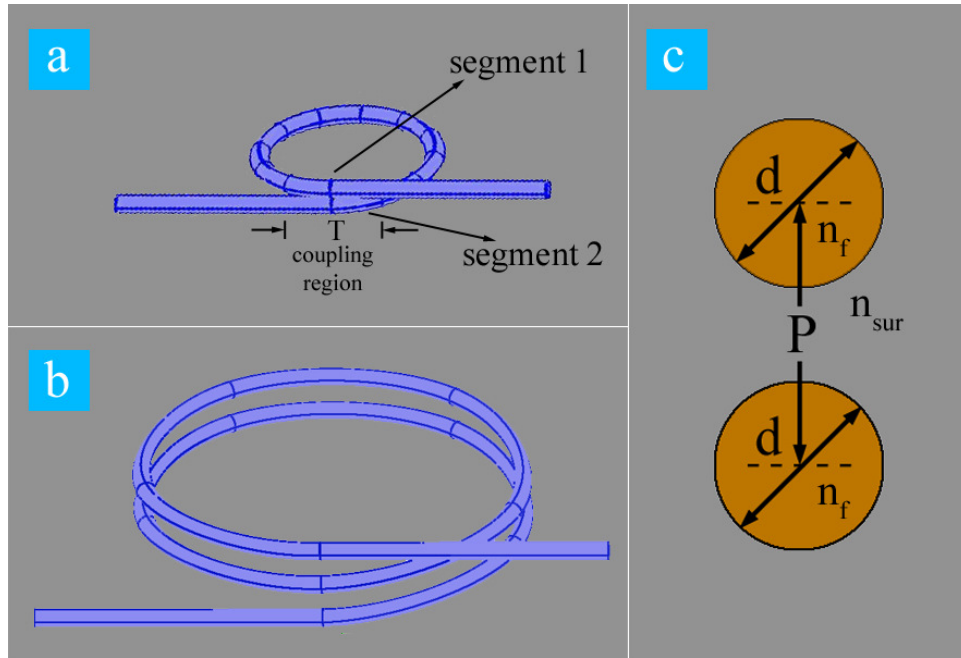


Fig. 1. (a) Basic configuration of an MFR, (b) basic configuration of a two-turn all-coupling 3D MCR, and (c) cross-section of a coupling region.

Here L and T are the loop length and coupling length, respectively. The ratio T/L ($0 \sim 1$) can be as large as 1 in a two-turn all-coupling MCR which is shown in Fig. 1(b). The cross-section of the MFR is also shown in Fig. 1(c). In our model, the coil is from a single uniform microfiber and has a shape close to a helix with a small pitch. We assume the diameter of the microfiber and the distance between the turns is uniform in our simulation. In that case the coupling coefficients between adjacent coils are the same. The input straight microfiber in fact is part of the first coil and the output microfiber is part of the last coil. And of course, the coupling on the input/output ends is the same because of the symmetric geometry. As the characteristic transversal dimension of the propagating mode is much smaller than the characteristic bend radius, then the adiabatic approximation of parallel transport can be applied [14, 17, 19]. The effective index, propagation constant and diameter are n_{eff} , β , and d , respectively. We use P ($= d$ in a loop/knot resonator, $\geq d$ in an MCR) to denote the pitch between the two segments in the coupling region, and n_f and n_{sur} to denote the refractive indices of the microfiber and environment (or analyte), respectively. Denoting the angular frequency as ω , the eigen modes in each segment before mode coupling are \mathbf{E}_p and \mathbf{H}_p ($p = 1, 2$), and the refractive index distribution of the entire coupled segment and each of the segments are N and N_p , respectively. The electromagnetic field amplitudes \mathbf{A} and \mathbf{B} in the two microfiber segments of the coupling region are related by the following coupled wave equations [20]:

$$\begin{cases} \frac{dA}{dz} + c_{12} \frac{dB}{dz} + j\chi_1 A + j\kappa_{12} B = 0 \\ \frac{dB}{dz} + c_{21} \frac{dA}{dz} + j\chi_2 B + j\kappa_{21} A = 0 \end{cases} \quad (1)$$

where

$$\begin{aligned}\kappa_{pq} &= \frac{\omega \varepsilon_0 \int_{-\infty}^{+\infty} \int_{-\infty}^{+\infty} (N^2 - N_q^2) E_p^* \cdot E_q dx dy}{\int_{-\infty}^{+\infty} \int_{-\infty}^{+\infty} u_z \cdot (E_p^* \times H_p + E_p \times H_p^*) dx dy} \\ c_{pq} &= \frac{\int_{-\infty}^{+\infty} \int_{-\infty}^{+\infty} u_z \cdot (E_p^* \times H_q + E_q \times H_p^*) dx dy}{\int_{-\infty}^{+\infty} \int_{-\infty}^{+\infty} u_z \cdot (E_p^* \times H_p + E_p \times H_p^*) dx dy} \\ \chi_p &= \frac{\omega \varepsilon_0 \int_{-\infty}^{+\infty} \int_{-\infty}^{+\infty} (N^2 - N_p^2) E_p^* \cdot E_p dx dy}{\int_{-\infty}^{+\infty} \int_{-\infty}^{+\infty} u_z \cdot (E_p^* \times H_p + E_p \times H_p^*) dx dy}\end{aligned}$$

Since MFRs are fabricated by one microfiber with self-coupling turns as shown in Fig. 1(a) and 1(b), we assume the two segments to be identical and we have $\kappa_{12} = \kappa_{21} = \kappa$, $c_{12} = c_{21} = c$ and $\chi_1 = \chi_2 = \chi$ because of the symmetric geometry.

The pair of p and q are either $(p, q) = (1, 2)$ or $(2, 1)$, and k is the coupling coefficient of the resonator.

In previous works, the coupled mode equation is often simplified as

$$\begin{cases} \frac{dA}{dz} + jkB = 0 \\ \frac{dB}{dz} + jkA = 0 \end{cases} \quad (2)$$

because c and χ are assumed to be zero. By solving Eq. (2), the following traditional resonance condition can be obtained:

$$\beta L = 2m\pi \quad m = 1, 2, 3, \dots \quad (3)$$

where β is the propagation constant. The resonant wavelength depends only on the effective index of the waveguide and is unrelated to the coupling effect.

However, if the diameter d of the microfiber and pitch P between the two segments are small enough, there will be a large evanescent field and a strong coupling effect. In order to investigate the resonator rigorously, we take c and χ into consideration, and by solving Eq. (1) we get

$$\begin{cases} A(z) = C_1 \exp[i(M + N)z] - C_2 \exp[i(M - N)z] \\ B(z) = C_1 \exp[i(M + N)z] + C_2 \exp[i(M - N)z] \end{cases} \quad (4)$$

where $M = \frac{\chi - kc}{c^2 - 1}$ and $N = \frac{k - c\chi}{c^2 - 1}$.

According to the boundary conditions, we get

$$\begin{cases} C_1 = \frac{1 - \exp[i(\lambda_2 T + \beta L)]}{\{2 - \exp[i(\lambda_1 T + \beta L)] - \exp[i(\lambda_2 T + \beta L)]\}} \\ C_2 = \frac{\exp[i(\lambda_2 T + \beta L)] - 1}{\{2 - \exp[i(\lambda_1 T + \beta L)] - \exp[i(\lambda_2 T + \beta L)]\}} \end{cases} \quad (5)$$

The modified resonance condition is

$$\beta L + MT = 2m\pi \quad m = 1, 2, 3 \dots \quad (6)$$

where β is the propagation constant. Compared to Eq. (3), the coupling effect is included in the resonance condition with an additional item MT . Next, we calculate the values of M to evaluate the importance of the coupling effect.

3. Simulation results

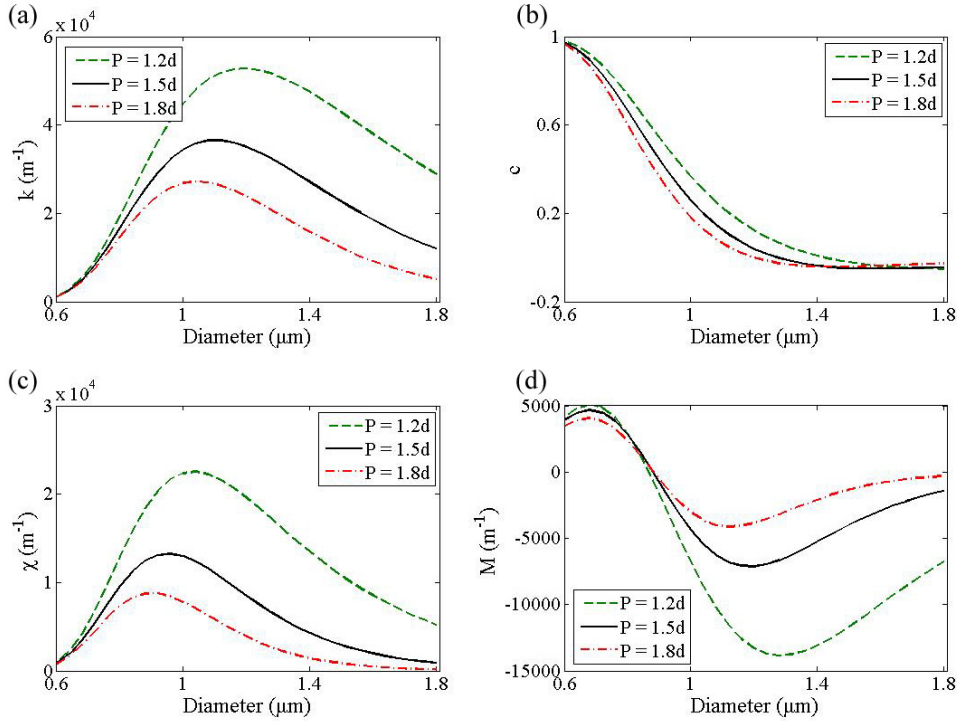


Fig. 2. The calculated (a) k , (b) c , (c) χ and (d) M profiles of a resonator with different diameter d and different pitch P .

In our simulations we assume $\lambda = 1.55 \mu\text{m}$, $n_f = 1.444$, $n_{\text{sur}} = 1.34$ for water and d ranges from 0.6 to 1.8 μm . We calculate the normalized frequency V according to $V = k_0 a (n_1^2 - n_2^2)^{1/2}$ and the fiber would be single-mode with $V < 2.405$ in those conditions. Thus, only the fundamental mode is excited at the input of the fiber and all the simulations in this paper are based on the fundamental mode. A full vector finite element method is used to calculate the dependence of the k , c and χ profiles on the fiber diameter d and the pitch P , respectively. According to these simulation values of k , c , and χ , we calculate the values of M with $M = \frac{\chi - kc}{c^2 - 1}$, which are plotted in Fig. 2(d). In previous works, c and χ are assumed to be zero, leading to the condition of $M = 0$. However, according to our simulation results from Fig. 2(d), the value of M can be as

large as $-13,844 \text{ m}^{-1}$ at $d = 1.28 \text{ }\mu\text{m}$ and $P = 1.2d$. Thus, M cannot be ignored, especially when the pitch P is relatively small.

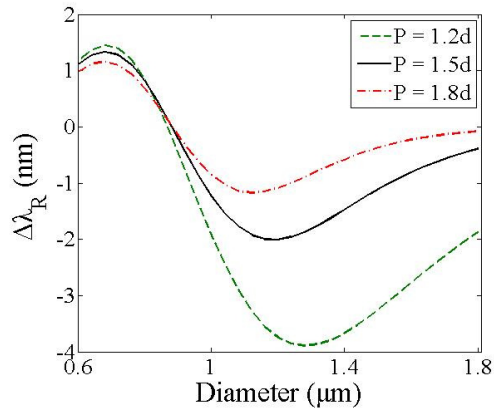


Fig. 3. Calculated $\Delta\lambda_R$ profiles of an MFR for different values of diameter d and pitch P .

Because of the additional term MT in our model, the resonant wavelength is modified by $\Delta\lambda_R = \lambda_R(M/\beta) \cdot \alpha$. Here $\alpha = T/L$ ($0 < \alpha \leq 1$) is the ratio of the coupling length to the ring length. In an all-coupling MCR, $\alpha = 1$.

In Fig. 3 we plot the values of $\Delta\lambda_R$ at different P and d . According to our simulation results, the difference in the resonant wavelength between our model and previous results can be up to -3.89 nm for $d = 1.28 \text{ }\mu\text{m}$, $P = 1.2d$, and $\lambda \approx 1550 \text{ nm}$. As the typical free spectral range is several nanometers, the resonant wavelength shift caused by the coupling effect cannot be ignored. Furthermore, our work also suggests a possible method to control the resonant wavelength by varying the pitch P and the diameter d . In particular, the pitch between adjacent turns in an MCR may change in response to external vibration or pressure. Thus, the MCR can be used as a vibration or pressure sensor and can also be tuned by the alternative external tuning technique of controlling the pitch and coupling strength.

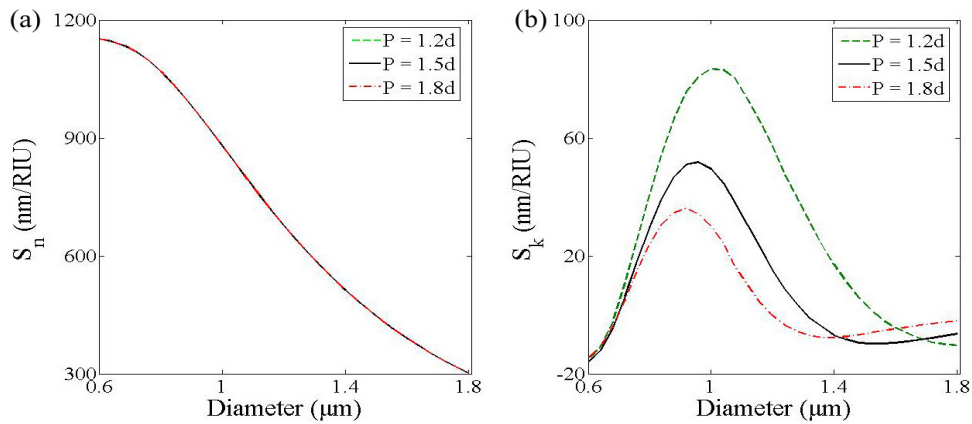


Fig. 4. Calculated (a) S_n and (b) S_k profiles of an MFR with different values of diameter d and pitch P .

MFRs have been widely used as refractometric sensors because of the large evanescent field. The sensitivity of an MFR is usually defined by the shift of the resonant wavelength as a function of the index change of the surrounding medium.

$$S = \frac{\partial \lambda_R}{\partial n_{sur}} \quad (7)$$

Here, λ_R is the resonant wavelength and n_{sur} is the refractive index of the surrounding medium. By including the resonance condition $\beta L + MT = 2m\pi$ in Eq. (7), we obtain

$$S = \frac{\partial \lambda_R}{\partial n_{sur}} = S_n + S_k \quad (8)$$

where

$$\begin{cases} S_n = \frac{2\pi}{\beta} \frac{\partial n_{eff}}{\partial n_{sur}} \\ S_k = \alpha \frac{\lambda}{\beta} \frac{\partial M}{\partial n_{sur}} \end{cases} \quad (9)$$

Here, S_n and S_k are the contributions of the evanescent field and the coupling effect, respectively.

In the traditional theory of previous literature, only S_n is considered. It can be seen from the formula that the values of S_n are only dependent on the change of the propagation constant and is not dependent on the coupling, as mentioned above. We can see from Fig. 4(a) that S_n drops with an increase in the diameter of the microfiber. This is because the intensity of the evanescent field and the coupling between the two segments both decay. As can be seen from Fig. 4(b), the values of S_k can be as large as 83 nm/RIU at $d = 1.04 \mu\text{m}$ and $P = 1.2d$, whereas the value of S_n is 836 nm/RIU for the same parameters, according to our simulation results. This implies that the sensitivity caused by the coupling effect can be up to 10% of the total sensitivity.

Clearly, with such a high value for S_k , the coupling strength greatly influences the sensitivity and should be taken into account when designing and analyzing an MFR.

4. Discussion and conclusion

For simplicity, we only considered the loop/knot MFR and two-turn MCR with simple two-wave coupling equations, which are very similar and agree with the model as shown in Fig. 1(a). Multi-turn MCRs are more complicated because of multi-resonant conditions and cross-coupling between different turns. However, our results and conclusions are also expected to be applicable to multi-turn MCRs.

In practice, the coupling intensity and the propagation constant may fluctuate with the change of the diameter of the microfiber and the distance between the turns. However, as our theoretical analysis is based on the average parameters of the MFR and the coupling length is relatively long, we believe our simulation results are applicable. Moreover, although we do not discuss the Q-factor which relates to the detection limit, the coupling also has a great contribution to the Q-factor.

In conclusion, by deriving fully coupled wave equations, we modify the previous theory on the resonance condition and sensitivity of an MFR. Our simulation results show that the resonant wavelength and sensitivity strongly depend on the coupling effect, which has been disregarded to date. Taking coupling into account, the resonant wavelength can be shifted by as

much as 3.89 nm and the sensitivity can be modified by as much as 83 nm/RIU. These effects are significant and useful in the design and applications of MFR sensors. In particular, the MCR may be employed as a vibration or pressure sensor and can be tuned by the alternative tuning technique of controlling the pitch and coupling strength suggested by this work.

Acknowledgments

This work was supported by the National 973 program under contract nos. 2011CBA00200, 2012CB921803, and 2010CB327800 and the NSFC program under contract nos. 11074117 and 60977039. The authors also acknowledge the support from PAPD and the Fundamental Research Funds for the Central Universities.